

Supporting Information

New insights on the defect sites evolution during CO oxidation over doped ceria nanocatalysts probed by in situ Raman spectroscopy

Enrico Sartoretti^{a,†}, Chiara Novara^{a,†}, Marco Fontana^b, Fabrizio Giorgis^a, Marco Piumetti^a, Samir Bensaid^{a,*}, Nunzio Russo^a, Debora Fino^a

^a Department of Applied Science and Technology, Politecnico di Torino, Corso Duca degli Abruzzi, 24, 10129 Turin, Italy.

^b Center for Sustainable Future Technologies, Istituto Italiano di Tecnologia, Via Livorno, 60, 10144 Turin, Italy.

*E-mail: samir.bensaid@polito.it

Experimental

Raman analyses

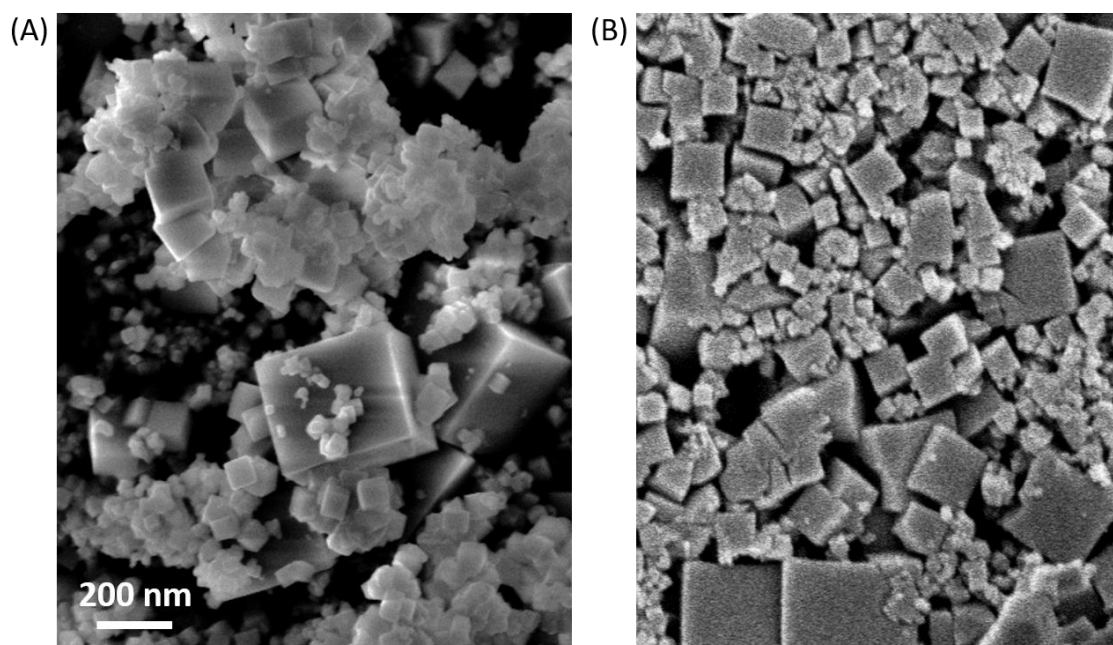


Fig. S1. FESEM micrographs of the CeO₂ catalyst in powder (A) and after compression at 3 bar to prepare a tablet (B). The images show no significant morphological changes due to the applied pressure.

Results and Discussion

Catalyst characterization and activity

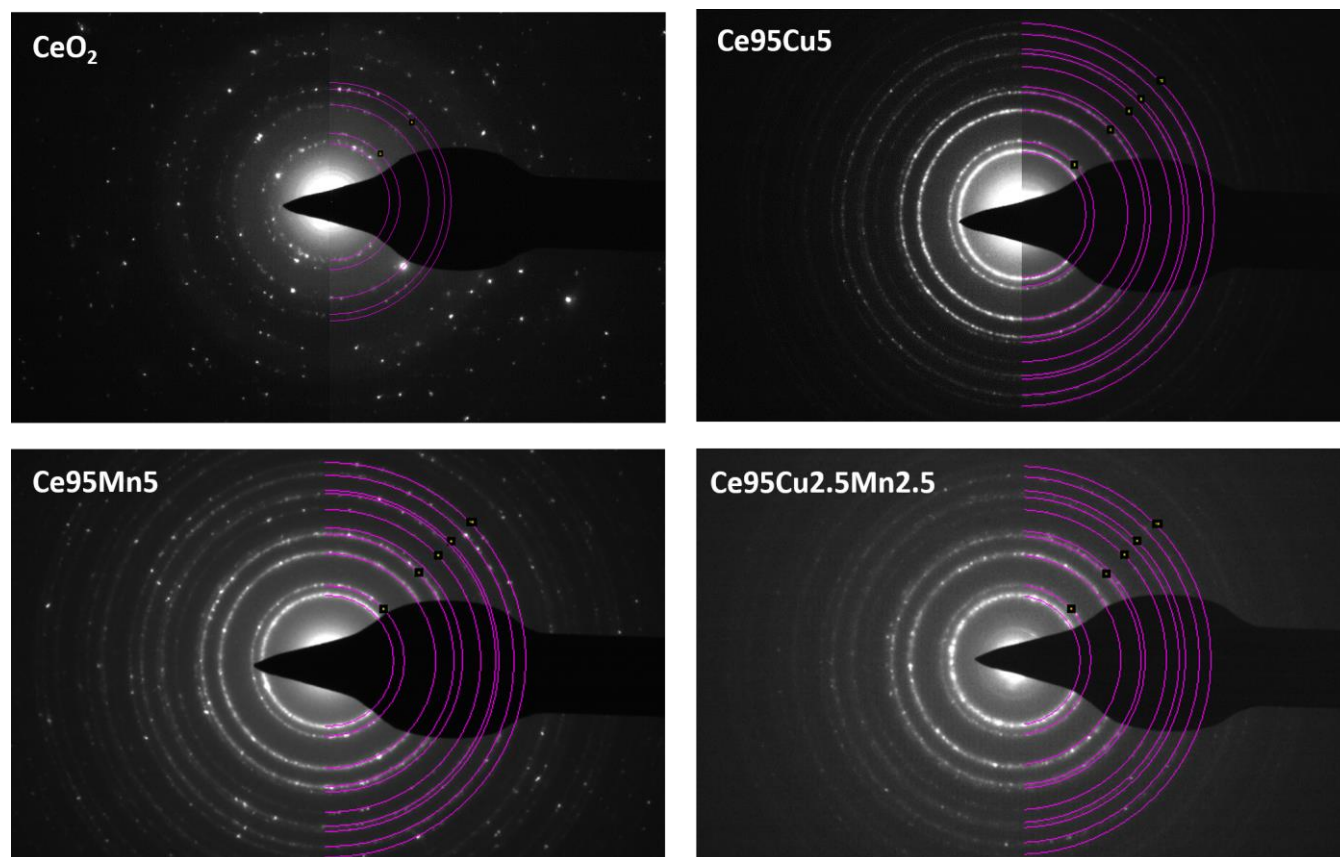


Fig. S2. Selected area electron diffraction (SAED) patterns of the four different samples. The violet lines represent a simulated pattern for ceria crystal structure.

Table S1 provides results obtained by the analysis of the electron diffraction patterns reported in Fig. S2. The diffraction rings were analyzed with the Circular Hough analysis tool [1] provided in Digital Micrograph™ software. The CeO₂ reference crystallographic structure (CeO₂ REF in the table) is calculated from data provided in [2].

Table S1. Summary of the results from SAED measurements on the four different classes of samples.

CeO ₂ REF	Miller indices	d (Å)	d/ d(111)		CeO ₂	ring	d/ d(111)		Ce95Mn5	ring	d/ d(111)
	(111)	3,12	1,00			1	1,00			1	1,00
	(200)	2,70	0,87			2	0,86			2	0,87
	(220)	1,91	0,61			3	0,61			3	0,61
	(311)	1,64	0,52			4	0,52			4	0,52
	(222)	1,56	0,50			5	0,49			5	0,50
					Ce95Cu5	ring	d/ d(111)		Ce95Cu2.5Mn2.5	ring	d/ d(111)
						1	1,00			1	1,00
						2	0,87			2	0,87
						3	0,61			3	0,61
						4	0,52			4	0,52
						5	0,50			5	0,50

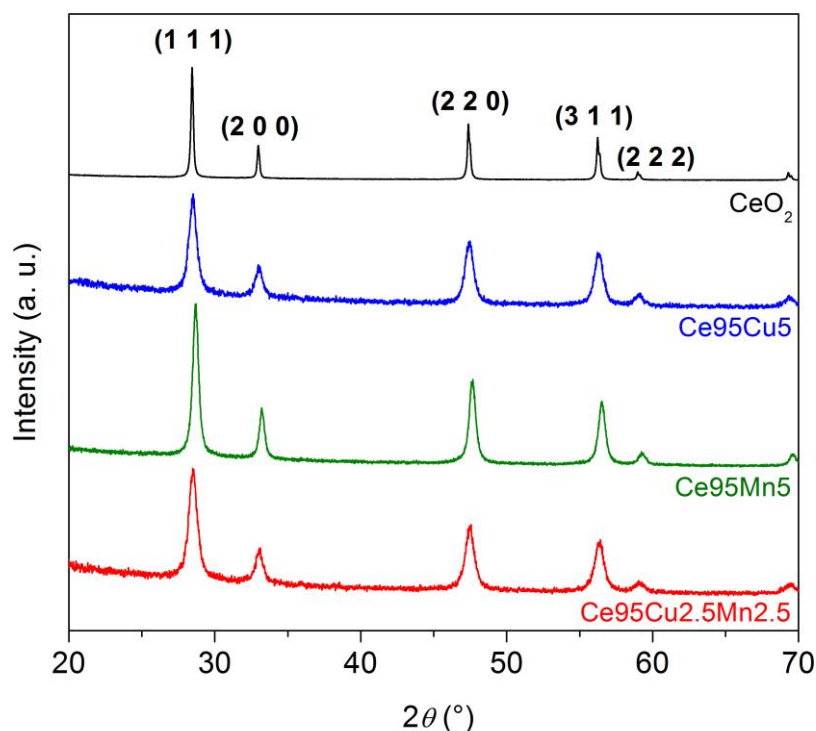


Fig. S3. XRD diffractograms of the four samples (data, except for Ce95 Mn5, and details about the experimental procedures previously reported in [3]). Powder XRD was performed in a Philips X'Pert PW3040 diffractometer, using a Cu $K\alpha$ radiation (wavelength $\lambda = 1.5418 \cdot 10^{-10}$ m, 2θ range = 20° – 70° ; step = 0.05° 2θ ; time per step = 0.2 s). The diffraction peaks were indexed according to the Powder Data File database (PDF 2000, International Centre of Diffraction Data, Pennsylvania). The crystal average size D_c (nm) reported in the manuscript was estimated using Scherrer's equation, $D_c = 0.9 \lambda / (\beta \cos \theta)$, where 0.9 is the shape factor for spheres, λ is the Cu $K\alpha$ wavelength (nm), β is the full-width at half maximum FWHM (rad) and θ is the Bragg angle (rad). The FWHM data were previously corrected comparing them with those of a lanthanum hexaboride standard. The lattice parameter a was predicted using Nelson-Riley function.

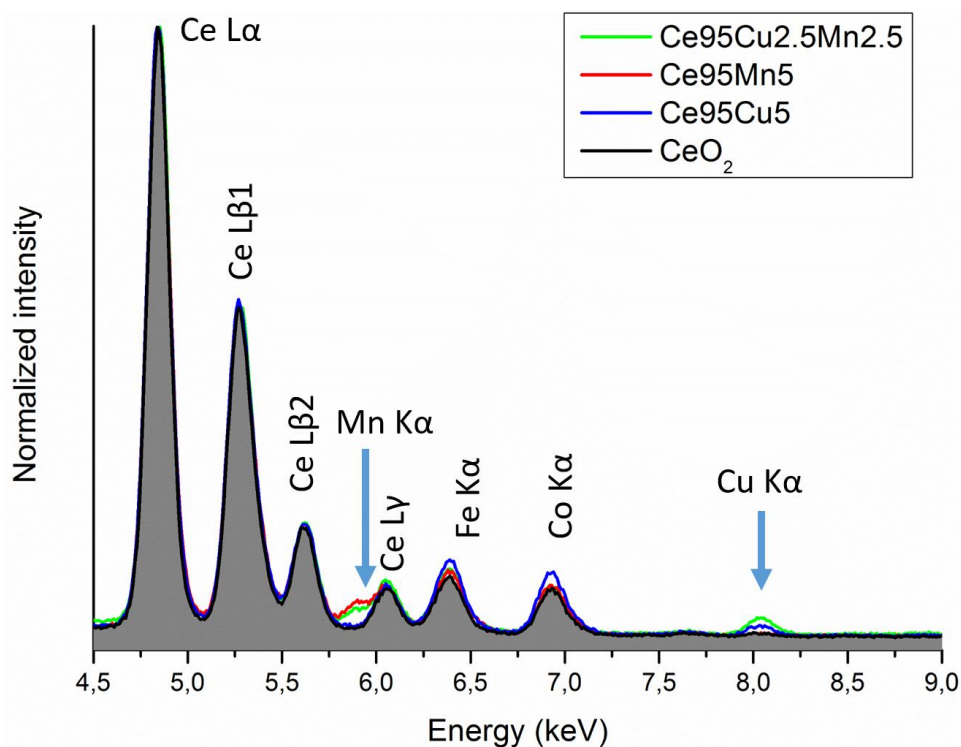


Fig. S4. Representative EDX spectra for the pristine and doped ceria powders acquired with parallel beam illumination in the transmission electron microscope.

Fig. S4 shows representative EDX spectra obtained with parallel beam illumination of the different pristine and doped ceria powders. These results confirm the presence of the dopant elements, in accordance with the specific precursors exploited for the synthesis. Au TEM grids were used for the analysis instead of common Cu grids, in order to avoid the presence of a spurious Cu $K\alpha$ peak. Fe/Co peaks are due to the pole pieces.

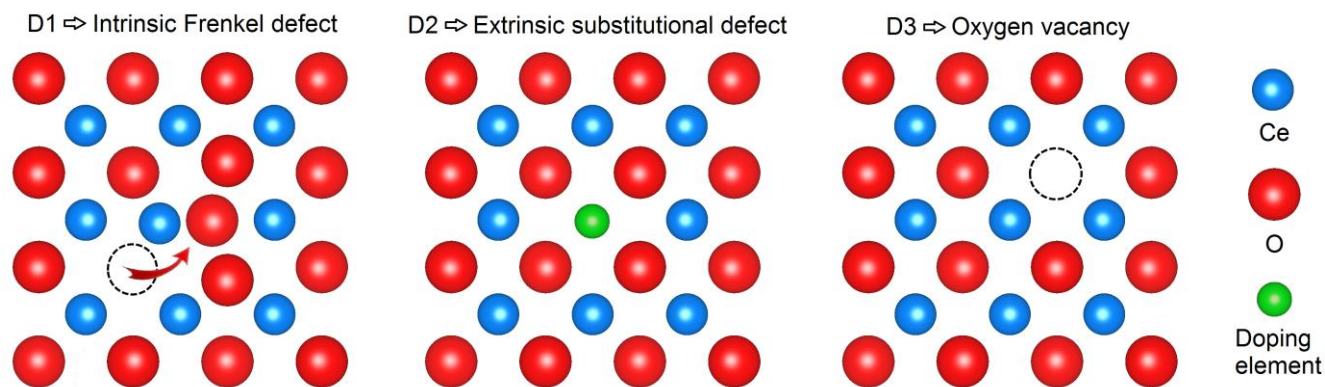


Fig. S5. Typical literature assignments of the observed Raman components to the different types of defect sites which can be found in the ceria lattice.

In situ Raman analyses of the CO oxidation reaction

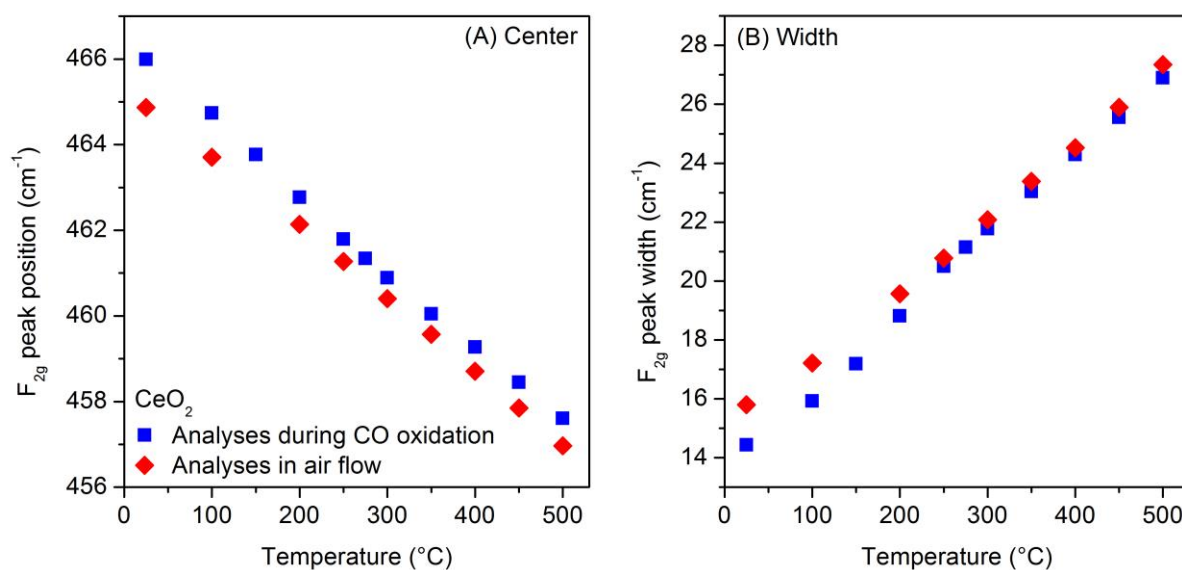


Fig. S6. Position (A) and full width at half maximum (B) of the F_{2g} peak as a function of the temperature. The values were obtained from the Raman spectra of pure CeO_2 collected during the in-situ analyses of CO oxidation (Fig. 4A) and during analyses in air flow [spectra reported in [4] (ref. [37] in the main text)].

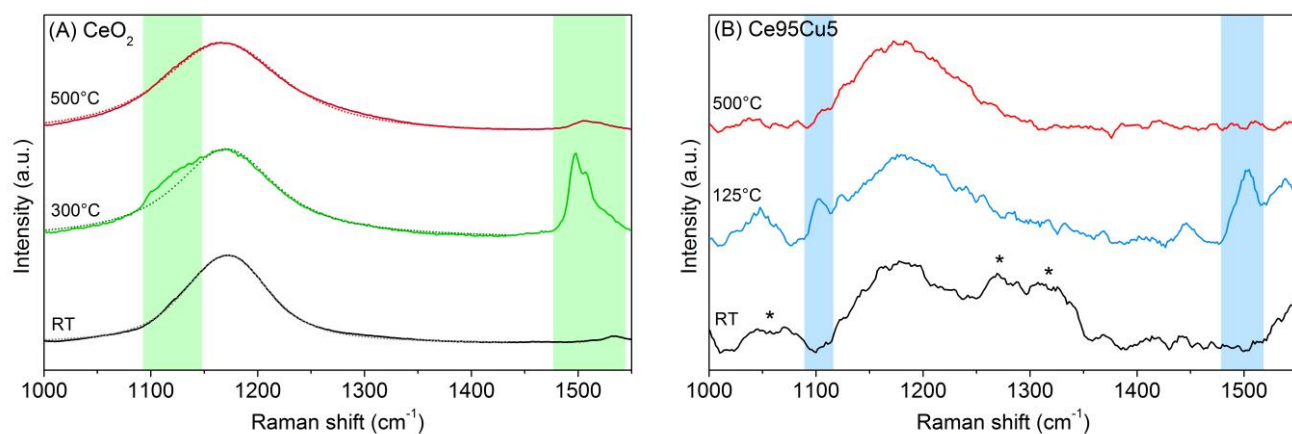


Fig. S7. Magnification in the 1000-1550 cm^{-1} range of the Raman spectra acquired on the CeO_2 (A) and $\text{Ce}_{95}\text{Cu}_5$ (B) samples while performing the CO oxidation from RT to 500 $^{\circ}\text{C}$. For each catalyst, the initial (RT) and final (500 $^{\circ}\text{C}$) spectra are reported, together with an intermediate spectrum recorded at the temperature at which the most intense polyenes-associated bands are visible (located in the regions highlighted with coloured bands). The dotted lines in the first figure, representing the shape of ceria second order band obtained by deconvolution, were added to assist the identification of the 1120 cm^{-1} band. The asterisks in Fig. S7B indicate peaks associated to the presence of contaminants at RT.

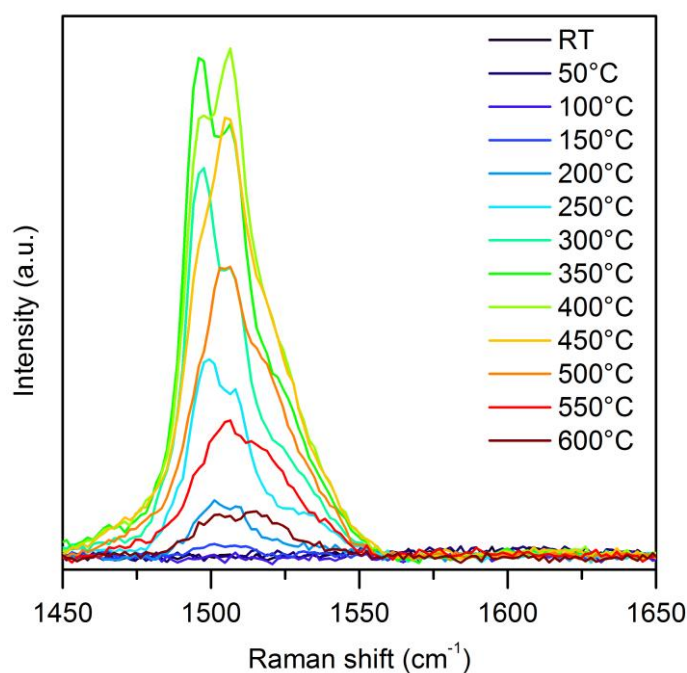


Fig. S8. Magnification in the 1450-1650 cm^{-1} range of the Raman spectra collected at different temperatures during the CO oxidation (1000 ppm of CO and 10% of O_2 in N_2) on a CeO_2 samples. The catalyst tablet was pretreated at 500 $^{\circ}\text{C}$ for 1 h before starting the analysis, in order to remove any organic contamination. Despite the absence of carbonaceous species at RT (no bands were detected in the 1450-1650 cm^{-1} range), the polyenes-related band located at about 1500 cm^{-1} appears and show a similar behaviour to that previously observed.

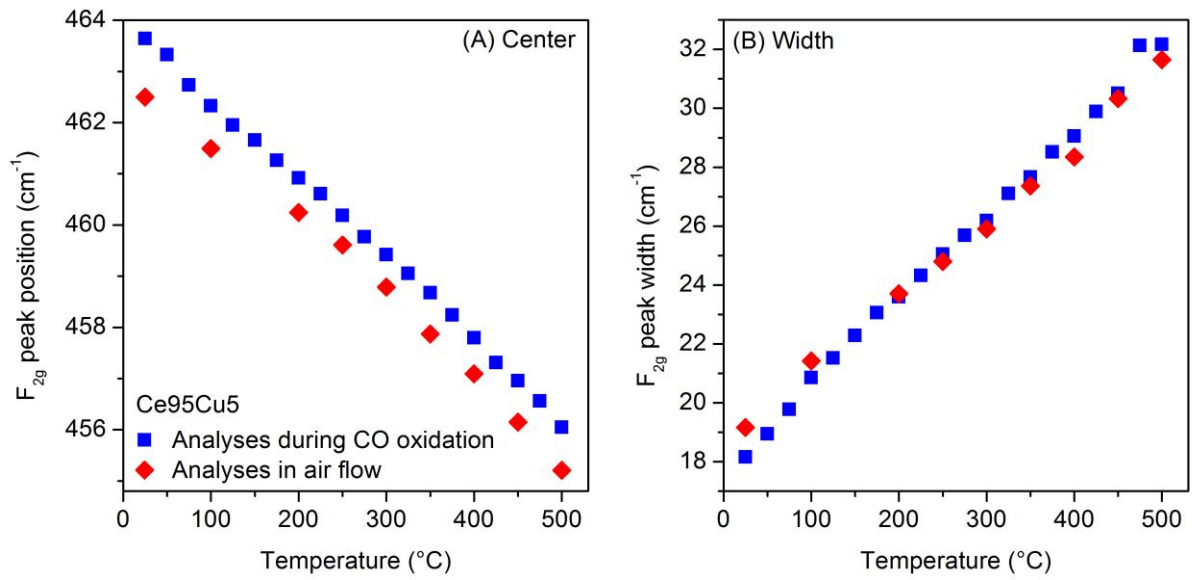


Fig. S9. Position (A) and full width at half maximum (B) of the F_{2g} peak as a function of the temperature. The values were obtained from the Raman spectra collected on $Ce_{95}Cu_5$ during the in-situ analyses of CO oxidation (Fig. 4B) and during analyses in air flow [spectra reported in [4] (ref. [37] in the main text)].

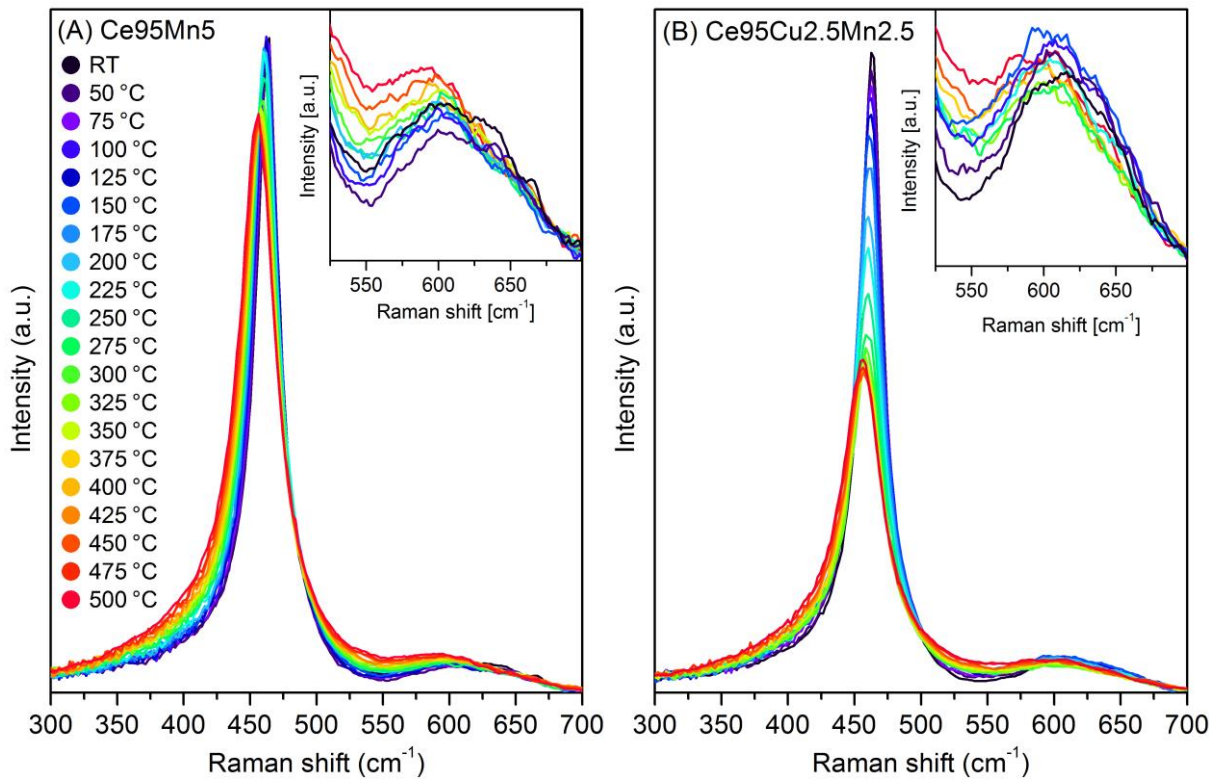


Fig. S10. Raman spectra collected at different temperatures during the CO oxidation on the $Ce_{95}Mn_5$ (A) and $Ce_{95}Cu_{2.5}Mn_{2.5}$ (B) samples. In the insets, the defect region is magnified (the spectra are shown every 50 $^{\circ}C$ to reduce the number of overlapping curves).

In situ Raman analyses during reduction-oxidation cycles

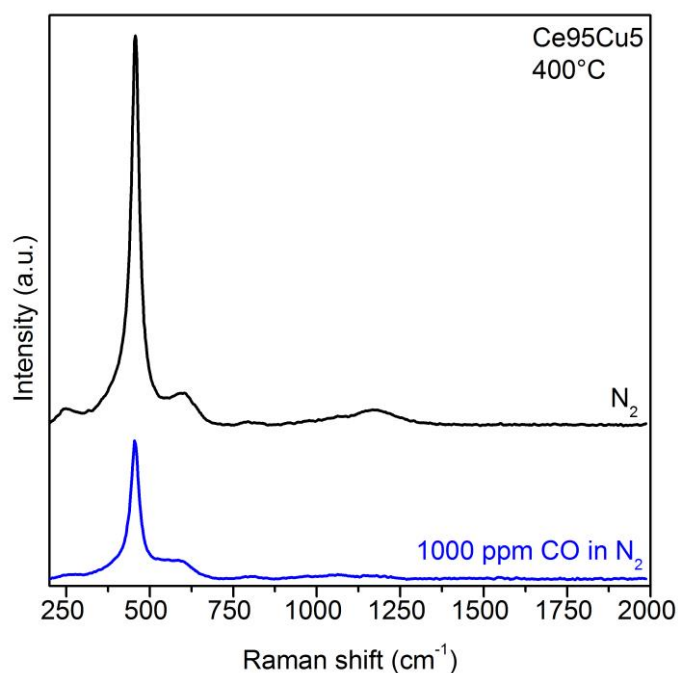


Fig. S11. Raman spectra acquired on the Ce₉₅Cu₅ sample at 400 °C in two different atmospheres during the cycles of reduction and oxidation. When the sample is exposed to 1000 ppm of CO in N₂, the spectral intensity drops but no bands related to the formation of soot-like species can be detected.

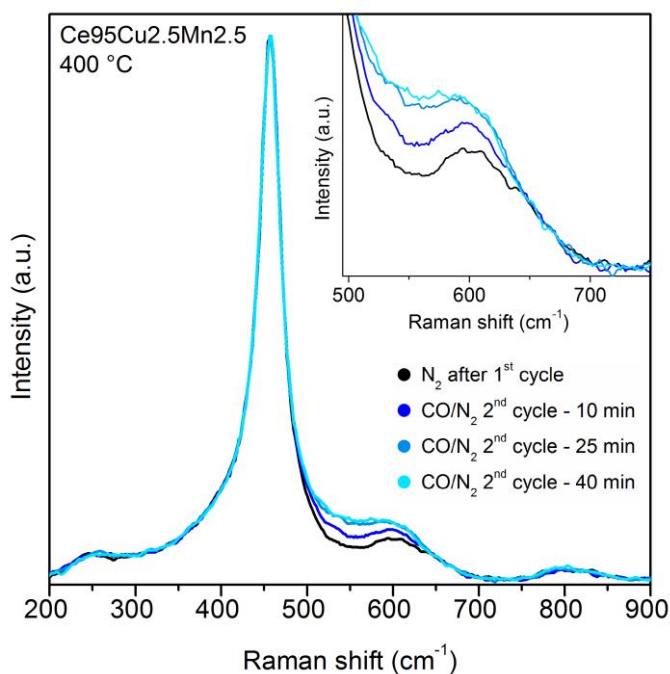


Fig. S12. Raman spectra acquired on the Ce₉₅Cu_{2.5}Mn_{2.5} sample during the reducing phase of the 2nd cycle of reduction and oxidation. The spectra were collected at 400 °C immediately before and 10, 25 and 40 min after the gas change from N₂ to the 1000 ppm CO/N₂ mixture. All the spectra were normalized to the intensity of the F_{2g} peak. In the inset a magnification of the defect band is shown.

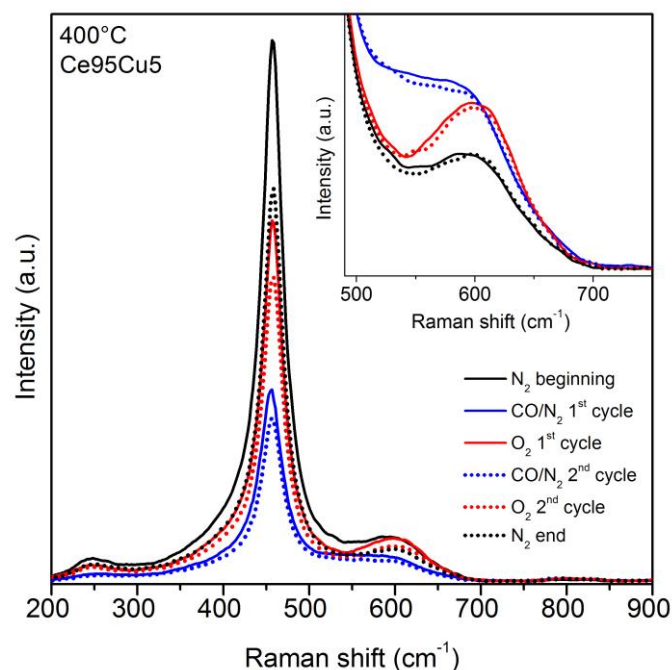


Fig. S13. Raman spectra acquired on the Ce95Cu5 sample at 400 °C during cycles of reduction and oxidation, in which 2000 ppm of CO in N₂ was used as reducing mixture. The spectra were collected 40 min after the gas change. In the inset the spectra normalized to the intensity of the F_{2g} peak are reported and a magnification of the defect band is shown.

References

- [1] D.R.G. Mitchell, Circular Hough transform diffraction analysis: A software tool for automated measurement of selected area electron diffraction patterns within Digital Micrograph™, *Ultramicroscopy*. 108 (2008) 367–374. doi:10.1016/j.ultramic.2007.06.003.
- [2] C. Artini, M. Pani, M.M. Carnasciali, M.T. Buscaglia, J.R. Plaisier, G.A. Costa, Structural features of Sm- and Gd-doped ceria studied by synchrotron X-ray diffraction and -raman spectroscopy, *Inorg. Chem.* 54 (2015) 4126–4137. doi:10.1021/acs.inorgchem.5b00395.
- [3] M. Dosa, M. Piumetti, S. Bensaid, T. Andana, C. Novara, F. Giorgis, D. Fino, N. Russo, Novel Mn–Cu-Containing CeO₂ Nanopolyhedra for the Oxidation of CO and Diesel Soot: Effect of Dopants on the Nanostructure and Catalytic Activity, *Catal. Letters*. 148 (2018) 298–311. doi:10.1007/s10562-017-2226-y.
- [4] E. Sartoretti, C. Novara, F. Giorgis, M. Piumetti, S. Bensaid, N. Russo, D. Fino, In situ Raman analyses of the soot oxidation reaction over nanostructured ceria-based catalysts, *Sci. Rep.* 9 (2019) 3875. doi:10.1038/s41598-019-39105-5.